Supplementary Information

Chomponoot Suppaso,[a] Chadawan Khamdang,[b] Likkhasit Wannasen,[c] Tomoki Kanazawa,[d] Akinobu Miyoshi,[e] Shunta Nishioka,[e] Kaewta Jetsrisuparb,[f] Sujitra Amnuaypanich,[a] Suwit Suthirakun,[b] Kazuhiko Maeda[e, *] and Nithima Khaorapapong[a, *]

[a]*Materials Chemistry Research Center, Department of Chemistry and Center of Excellence for Innovation in Chemistry, Faculty of Science, Khon Kaen 40002, Thailand*

[b]*School of Chemistry, Institute of Science, Suranaree University of Technology, Nakhon Ratchasima, Thailand 30000*

[c]*Nanotec-KKU Center of Excellence on Advanced Nanomaterials for Energy Production and Storage, Department of Physics, Faculty of Science, Khon Kaen University, Khon Kaen 40002, Thailand*

[d] *Institute of Materials Structure Science, High Energy Accelerator Research Organization, 1-1 Oho, Tsukuba, Ibaraki 305-0801, Japan.*

[e]*Department of Chemistry, Graduate School of Science and Engineering, Tokyo Institute of Technology, 2-12-1-NE-2 Ookayama, Meguro-ku, Tokyo 152-8550, Japan.*

[f]*Department of Chemical Engineering, Khon Kaen University, Khon Kaen 40002, Thailand*

Corresponding author

N.K. nithima@kku.ac.th,

K.M. maedak@chem.titech.ac.jp

Structural properties

Before the study properties of CuO (111), NiO (111), $NiFe_2O_4$ (311), and NiFe LDH (003), bulk structures are explored firstly, as shown in Fig. S1. CuO has a monoclinic structure, and the lattice constants a = 4.53 Å, b = 3.54 Å, c = 5.12 Å, and β = 99.19° are in good agreement with experimental values (a = 4.68 Å, b = 3.42 Å, c = 5.13 Å, and β = 99.53°).[1] NiO has a cubic structure, results in the optimized lattice constant of a = 4.16 Å, which compares favorably with the experimental value of a = 4.17 Å.[2] $NiFe_2O_4$ crystallizes in the α type inverse spinel, which has a tetragonal P4122/P4322 symmetry. Equal numbers of Ni and Fe atoms occupy octahedral sites, while the remaining Fe atoms occupy tetrahedral sites, the lattice constant has obtained a value of 8.10 Å compared to the experimental value was 8.33 Å.[3] NiFe LDH the lattice constants a = 12.21 Å, b = 6.10 Å, c = 22.40 Å, and the interlayer spacing is 8.54 Å with good agreement with the experiment value (8.29 Å).[4]

After complete optimization of bulk structures, slab models were studied, as shown in Fig. S2. CuO (111) 6 layers slab model with top three atomic layers are allowed to fully relax in all of the geometry optimization calculations and the 3 bottom layers are kept fixed, lattice constants were a = 5.75 Å, b = 6.22 Å, c = 27.56 Å, and β = 104.28° are good agreement with experimental values (a = 5.77 Å, b = 6.14 Å, and c = 23.07 Å).[5] NiO (111) 6 layers slab model with top 3 atomic layers are allowed to relax and the 3 bottom layers are fixed, the lattice constants were a = 5.88 Å, c = 21.00 Å, and γ = 60.00°. On the previous study of NiO (111) surface, there have studied on both oxygen- and metal-terminated surfaces of NiO (111), which find the O-terminated surface to be slightly more stable than the M-terminated surface, so we choose the O-terminated surface for NiO (111) in this study.[6] $NiFe_2O_4$ (311) surface using symmetric slabs of 12 layers with top 6 atomic layers are allowed to relax and the 6 bottom layers are fixed, the configurations we consider were O-termination, Fe-termination and Ni-termination, which the result shows that O-termination becomes most

stable surface for $NiFe_2O_4$ (311). Finally, NiFe LDH (003) surface model contain of one-layer metal hydroxides. The mole ratio of Ni and Fe in the original NiFe LDH (003) surface model is 3:1, the hydrogen atoms on the upper layer were removed for the adsorption of water and hydrogen intermediates.[7] All the slab models using the vacuum of 15.00 Å is employed, which can eliminate the interaction between surface slabs.

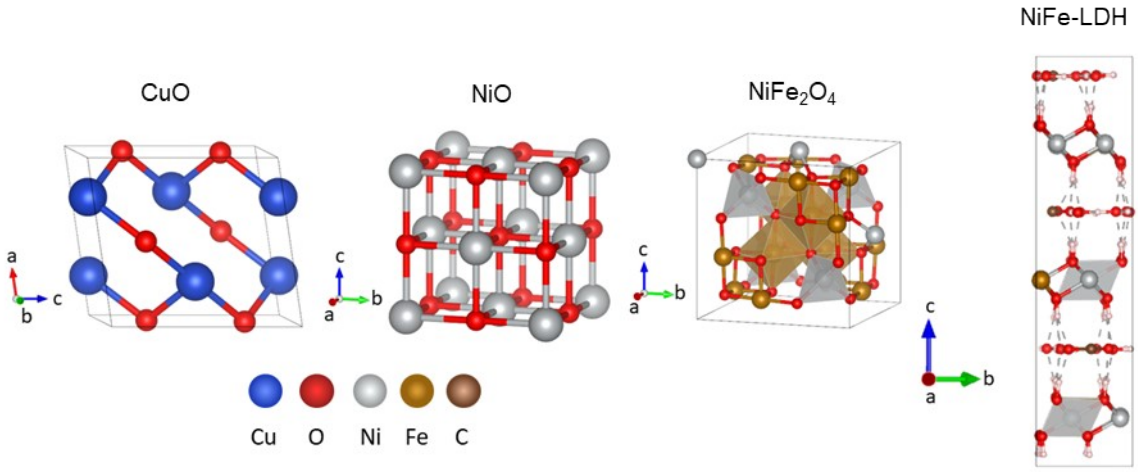

Fig. S1 The optimized bulk structure of (a) CuO, (b) NiO, (c) $NiFe_2O_4$, and (d) NiFe LDH.

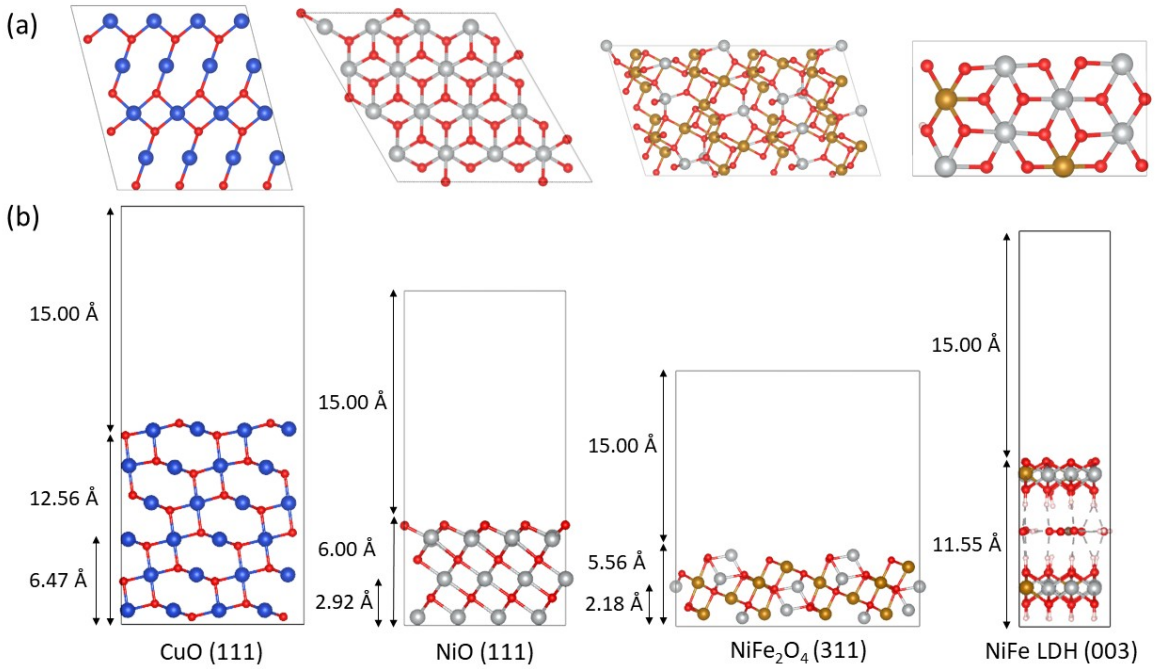

Fig. S2 a) top view and b) side view of slab models of CuO (111), NiO (111), $NiFe_2O_4$ (311), and NiFe LDH (003).

Energy diagram

Among the possible adsorption sites on the CuO (111), NiO (111), $NiFe_2O_4$ (311), and NiFe LDH (003) the most stable molecular adsorption of water and hydrogen co-adsorption are shown in Fig. S3. The adsorption energy, E_{ads}, is defined as

$$E_{ads} = E_{H*} - \left(E* + 1/2E_{H_2}\right)$$

where E_* and E_{H*} are the total energies of bare surface and adsorbed H atom on the surface, respectively; and E_{H2} is the total energy of an isolated H_2 molecule. The adsorption for H-O (O atom of the surface) with a distance of 1.00 Å.[8] In Fig. S3(a), the distance between H_2O and H adsorbed is 1.77 Å, and H_2O with surface O atom is 1.75 Å. In Figure 3b, the distance between H_2O and H adsorbed is 1.60 Å, and H_2O with surface O atom is 2.01 Å. In Fig. S3(c), the distance between H_2O and H adsorbed is 1.71 Å, and H_2O with surface O atom is 2.28 Å. In Figure S3(d), the distance between H_2O and H adsorbed is 1.78 Å, and H_2O with surface O atom is 2.01 Å. The adsorption energies of the four models are in the following order: (b) > (d) > (a) > (c) it is indicated that the NiO (111) surface was the most stable surface for water and hydrogen co-adsorption.

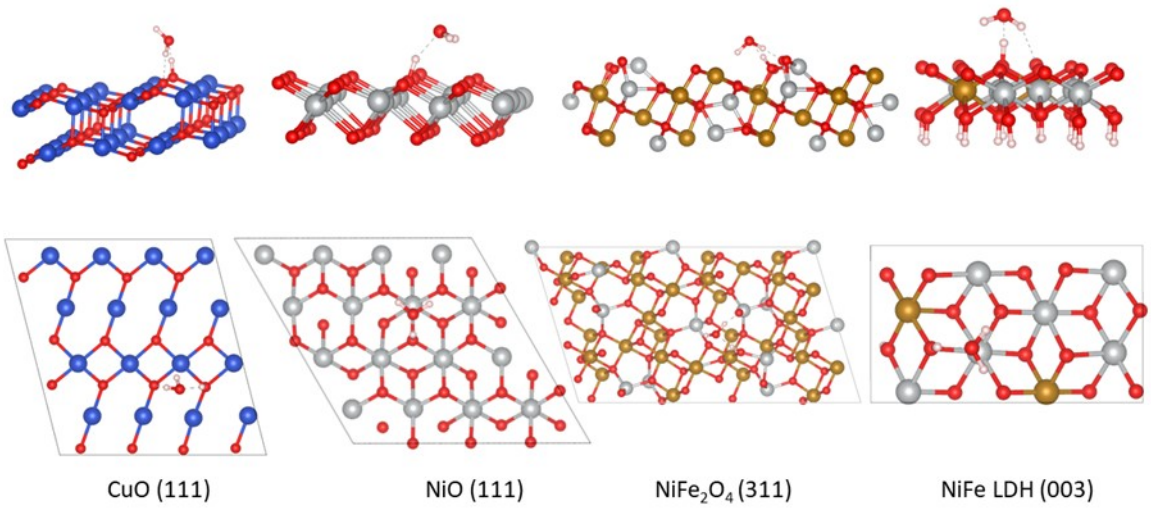

Fig. S3 Side view and top view of stable configuration for water and hydrogen co-adsorption on a) CuO (111), b) NiO (111), c) $NiFe_2O_4$ (001), and d) NiFe LDH (003).

The schematic of the HER activity of a given surface is determined through the free energy of adsorbed hydrogen under equilibrium conditions of the reaction. The adsorption free energy corresponding to the HER mechanism is defined as[9]

$$\Delta G_{H*} = E_{ads} + \Delta ZPE - T\Delta S$$

where E_{ads} signifies the adsorption energy of water and hydrogen co-adsorption, ΔZPE is the change in the zero-point energy (*ZPE*) of hydrogen in the adsorbed state and gas phase, and $T\Delta S$ represents the entropy difference of water and hydrogen co-adsorption in the adsorbed and gas state, i.e., vibration, rotation, and translation of gas-phase species; for adsorbed species, only vibrational contributions were considered since rotational and translational motions become frustrated. The *ZPE* correction was calculated according to

$$ZPE = \frac{hc}{2}\sum_{i}^{k}\frac{1}{\lambda_i}$$

where h is the Planck constant, c is the speed of light, λ_i the wavelength corresponding to the i-th vibrational mode, and k is the number of vibrational modes. The vibrational entropy S_{vib} was calculated assuming that each mode behaves like a harmonic oscillator, as shown in the following

$$S_{vib} = R\sum_{i}^{k}\left(\frac{x_i}{e^{x_i}-1} - \ln\left(1-e^{-x_i}\right)\right)$$

where, $x_i = \frac{hc}{k_B T}\frac{1}{\lambda_i}$, R is the ideal gas constant, k_B is the Boltzmann constant, and T the reaction temperature.[10]

Table S1 Calculated BET surface area of the as-prepared and calcined products.

Samples	BET surface area/ $m^2 g^{-1}$	
	As-prepared product	After calcination
NiFe-LDH	69	15
Composites		
-prepared by hydrothermal	44	25
-prepared by solid state reaction	41	23
-prepared by physical mixing	40	20
CuO	16	

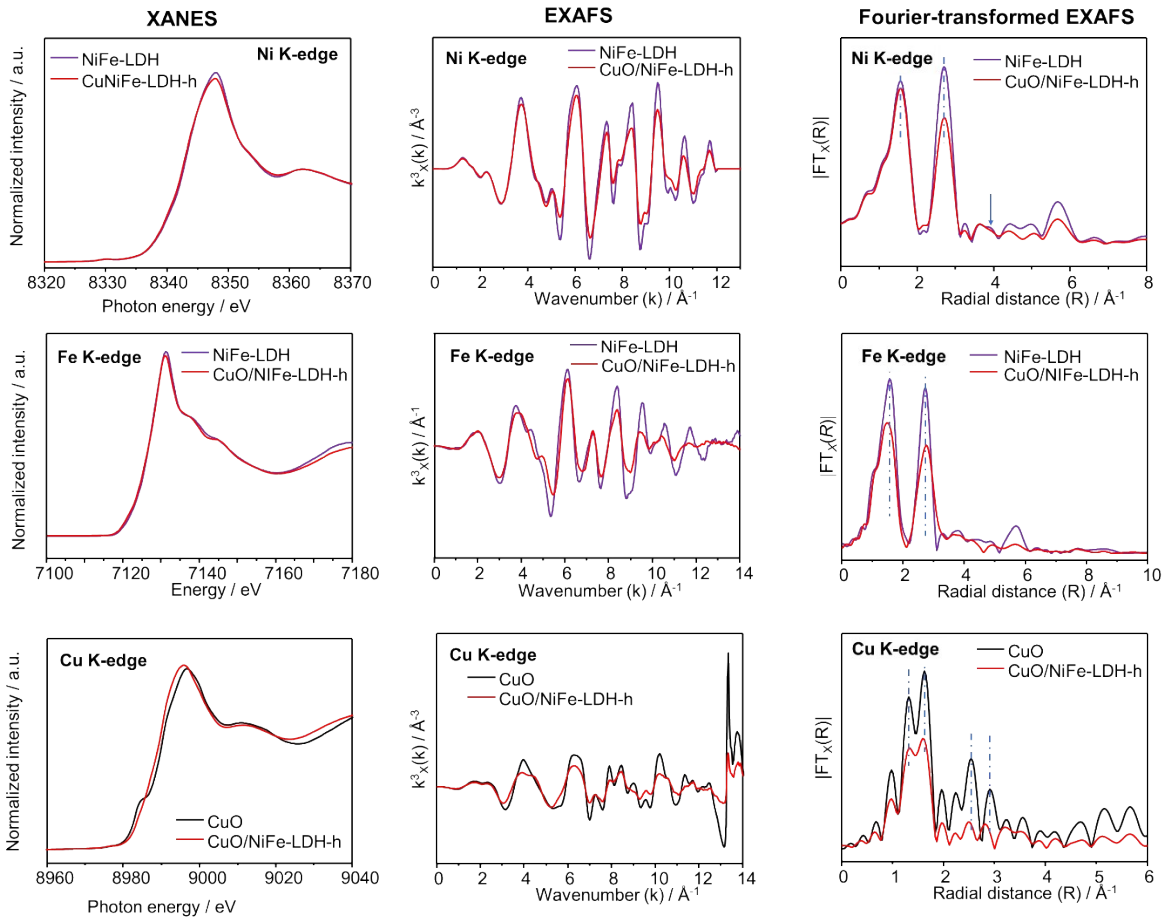

Fig. S4 The XAFS results including XANES (left), EXAFS (middle) and Fourier-transformed EXAFS (right) spectra of Ni K-edge (top), Fe K-edge (middle) and Cu K-edge (bottom) of the NiFe-LDH, CuO and CuO/NiFe-LDH-h.

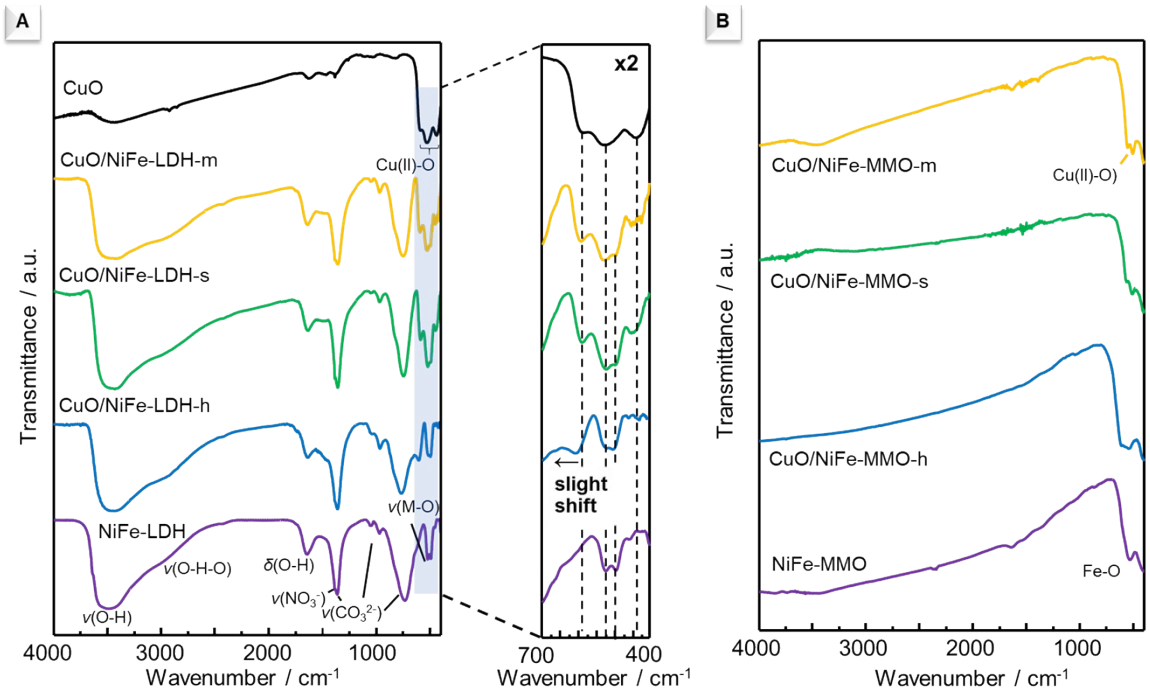

Fig. S5 FTIR spectra of CuO/NiFe-LDH composites (A) and their calcined products (B).

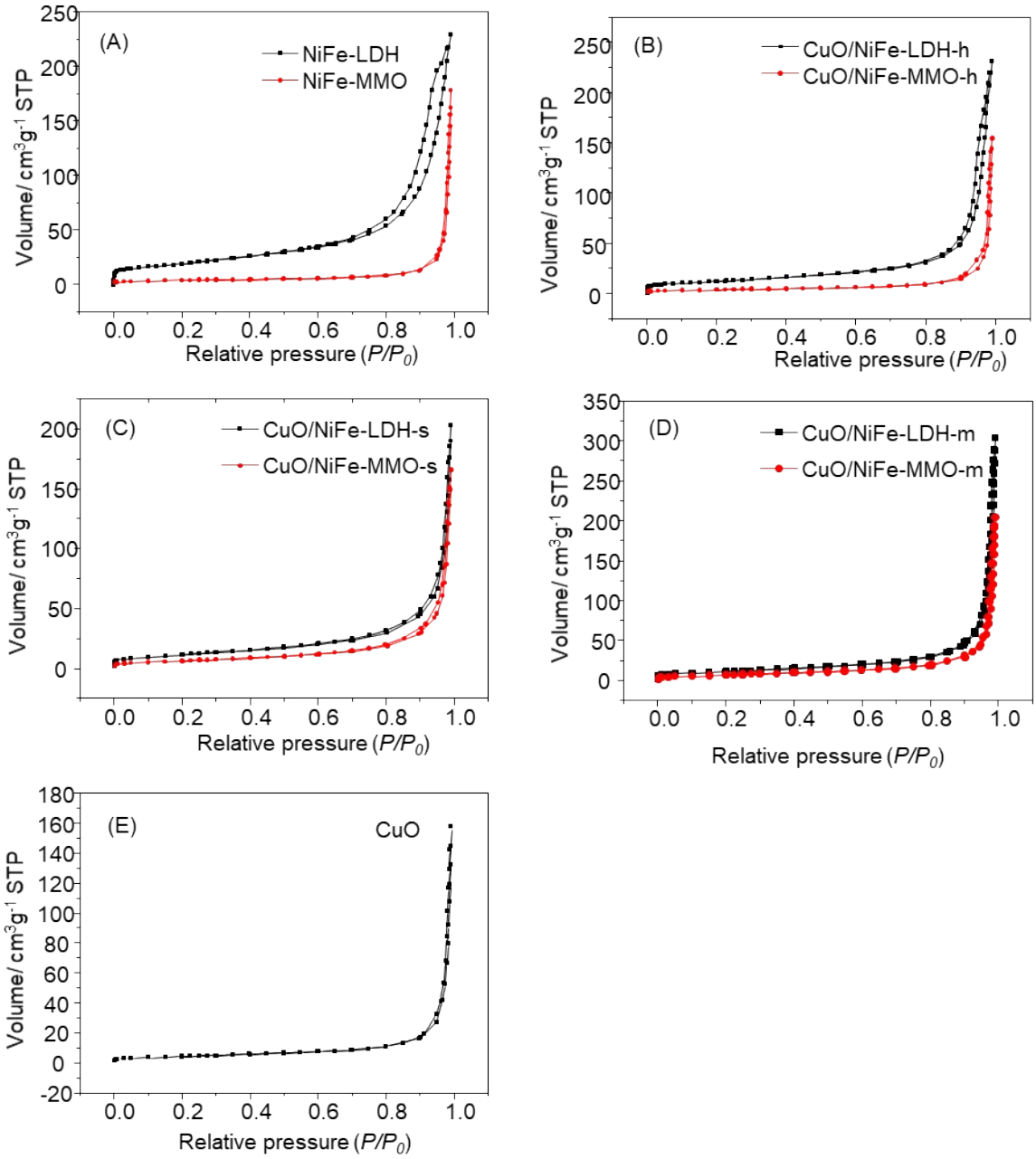

Fig. S6 N_2 adsorption-desorption isotherms of (A) pristine NiFe-LDH, CuO/NiFe-LDH composite prepared by (B) hydrothermal, (C) solid-state reaction and (D) physical mixing and (E) pure CuO.

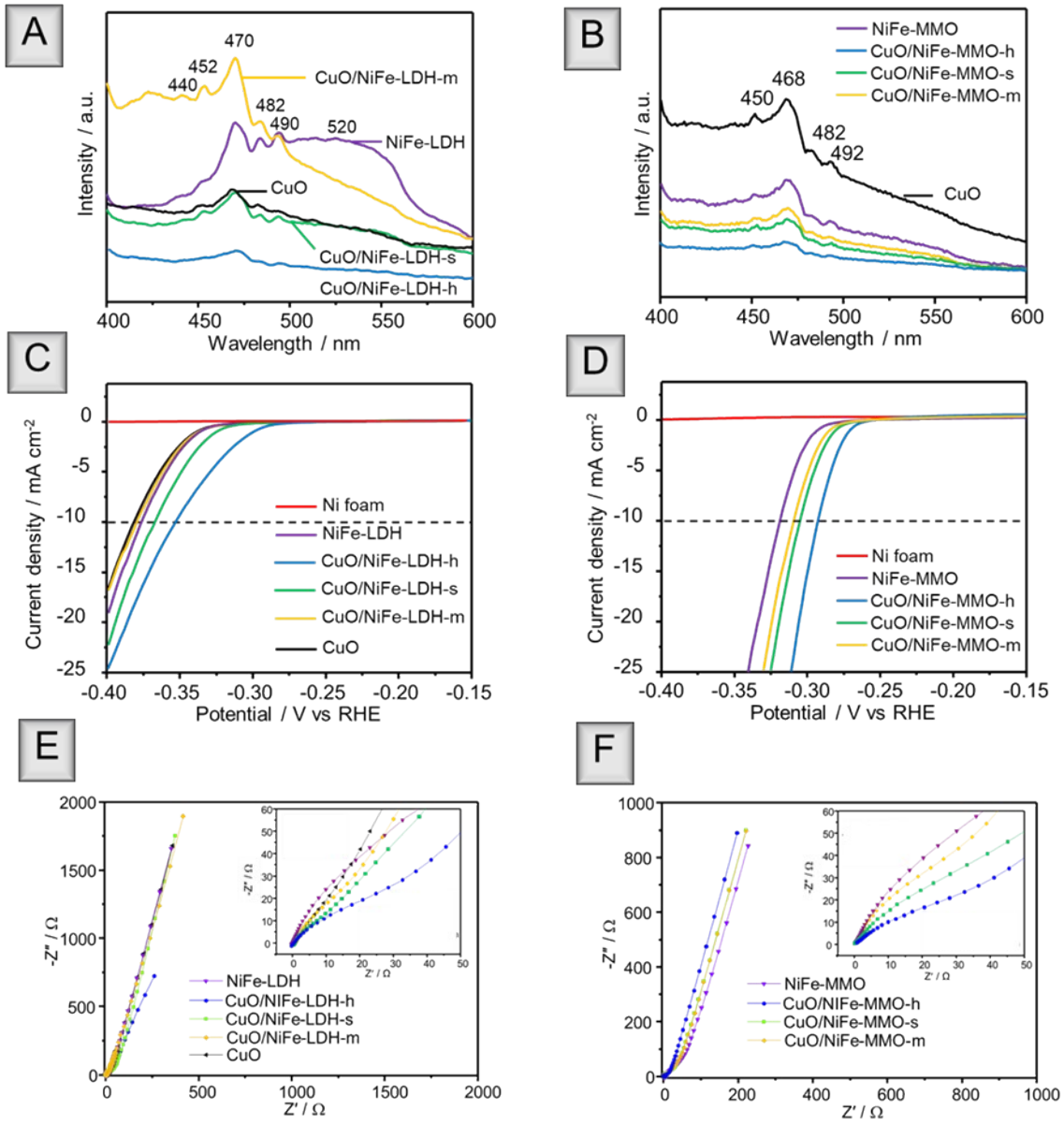

Fig. S7 (A, B) PL emission spectra with an excitation wavelength of 350 nm, (C, D) LSV spectra and (E, F) Nyquist plots of CuO/NiFe-LDH composites (left) and their calcined products (right). The EIS data were fitted to equivalent circuit model according to the previous report[11].

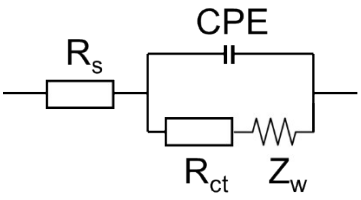

where R_s and R_{ct} represent bulk electrolyte and charge transfer resistances, respectively. The constant phase element or CPE equals to a double-layer capacitance, while, Warburg impedance or Z_w represents the diffusion of the ion in an electrolyte.

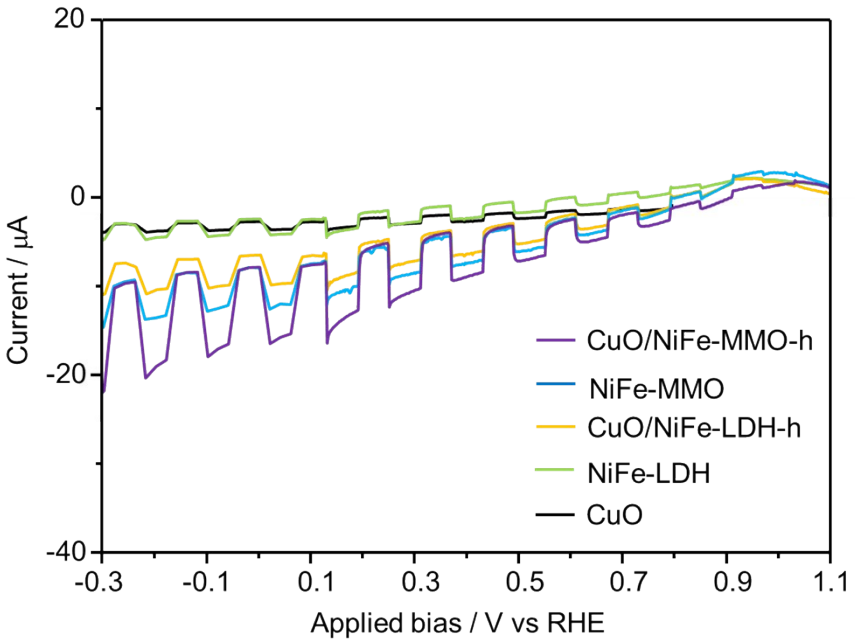

Fig. S8 Linear sweep voltammetry of prepared sample/FTO electrodes under visible-light chopped illumination (300 W Xe lamp, λ > 400 nm) in 0.1 M Na_2SO_4 solution.

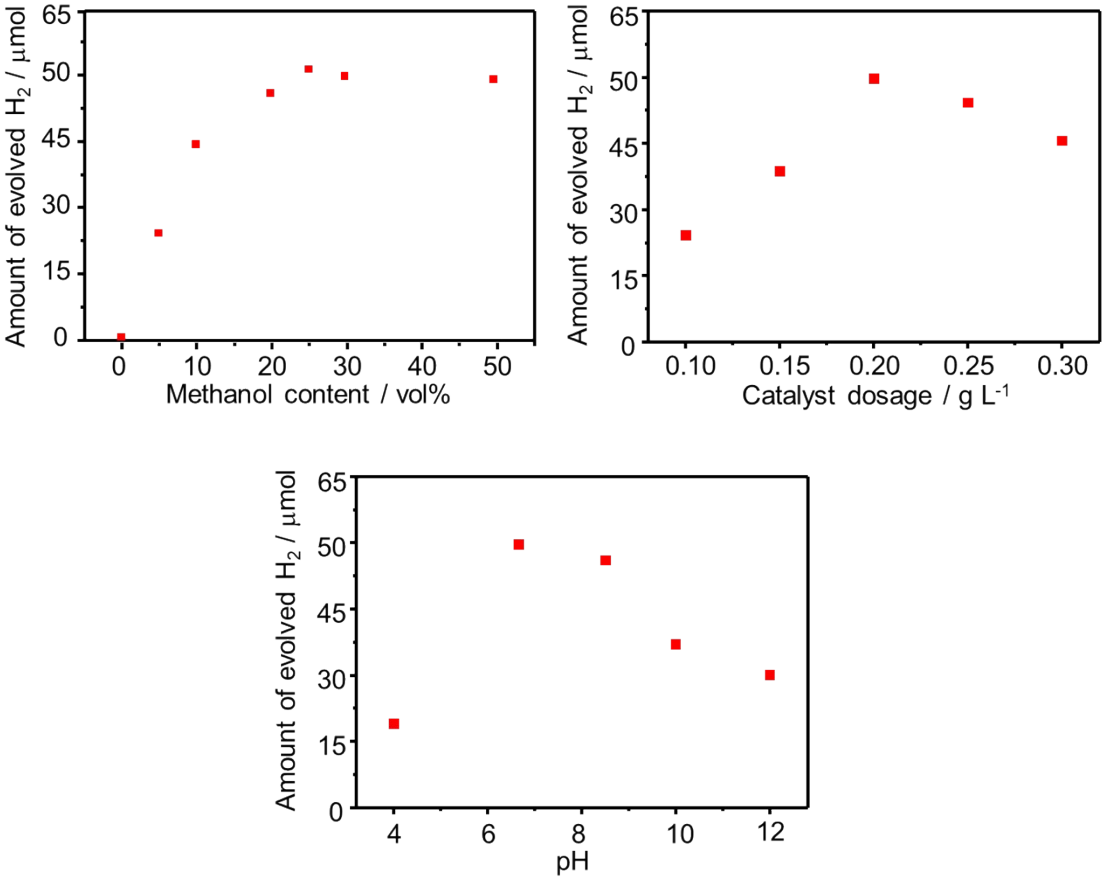

Fig. S9 Effect of methanol concentration (left), catalyst dosage (right) and pH (centre) on the photocatalytic H_2 production over CuO/NiFe-MMO-h. Reaction conditions: catalyst, 50, 75, 100, 125 and 150 mg; 0-50 %vol methanol aqueous solution, 500 mL; light source, high pressure mercury lamp (100 W, HL-100, SEN LIGHTS Corporation, $\lambda \approx 250$-580 nm); irradiation time, 6 h.

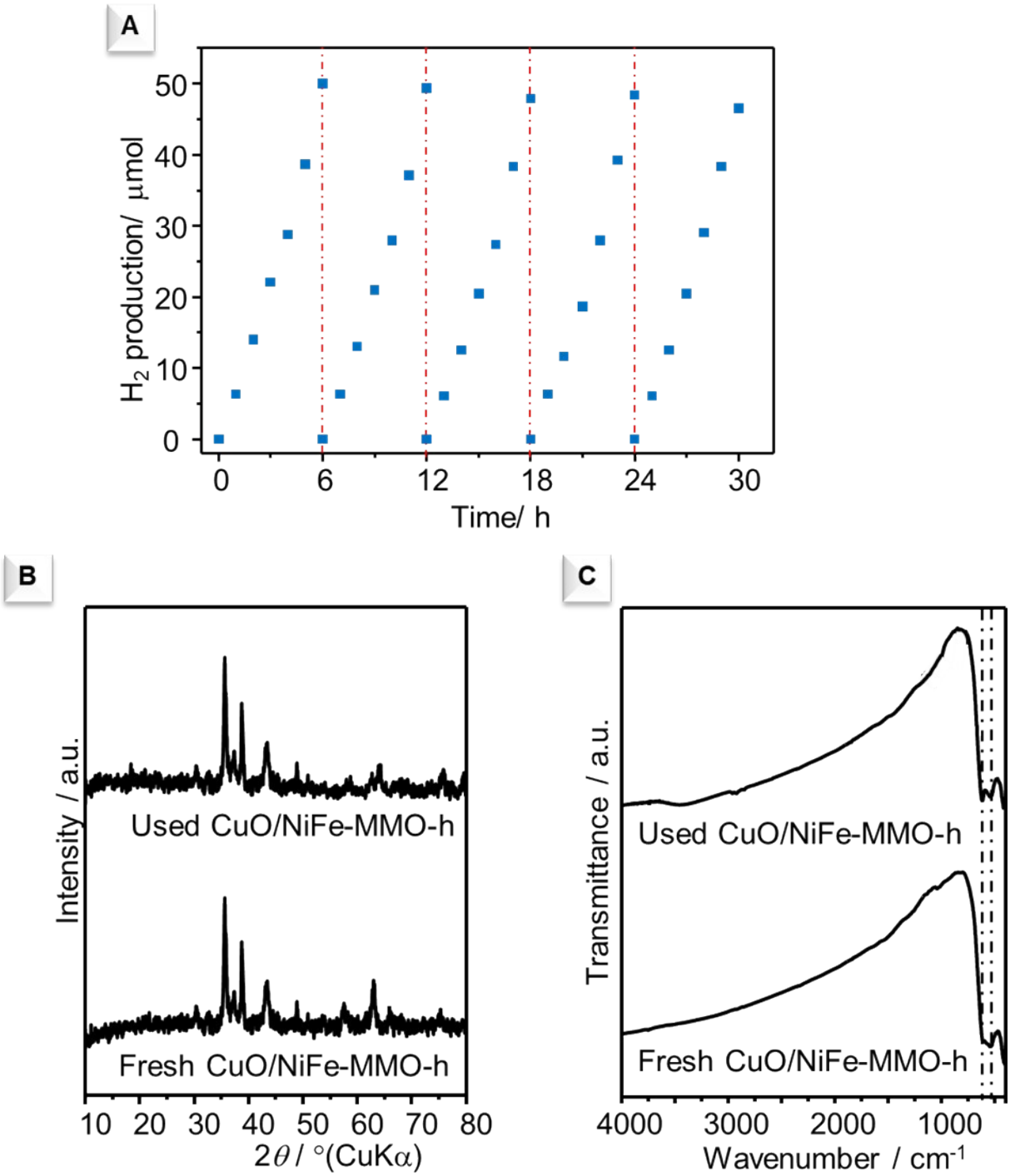

Fig. S10 (A) Photocatalytic cycling test, (B) FTIR spectra and (C) XRD patterns of CuO/NiFe-MMO-h before and after photocatalytic H_2 production reaction.

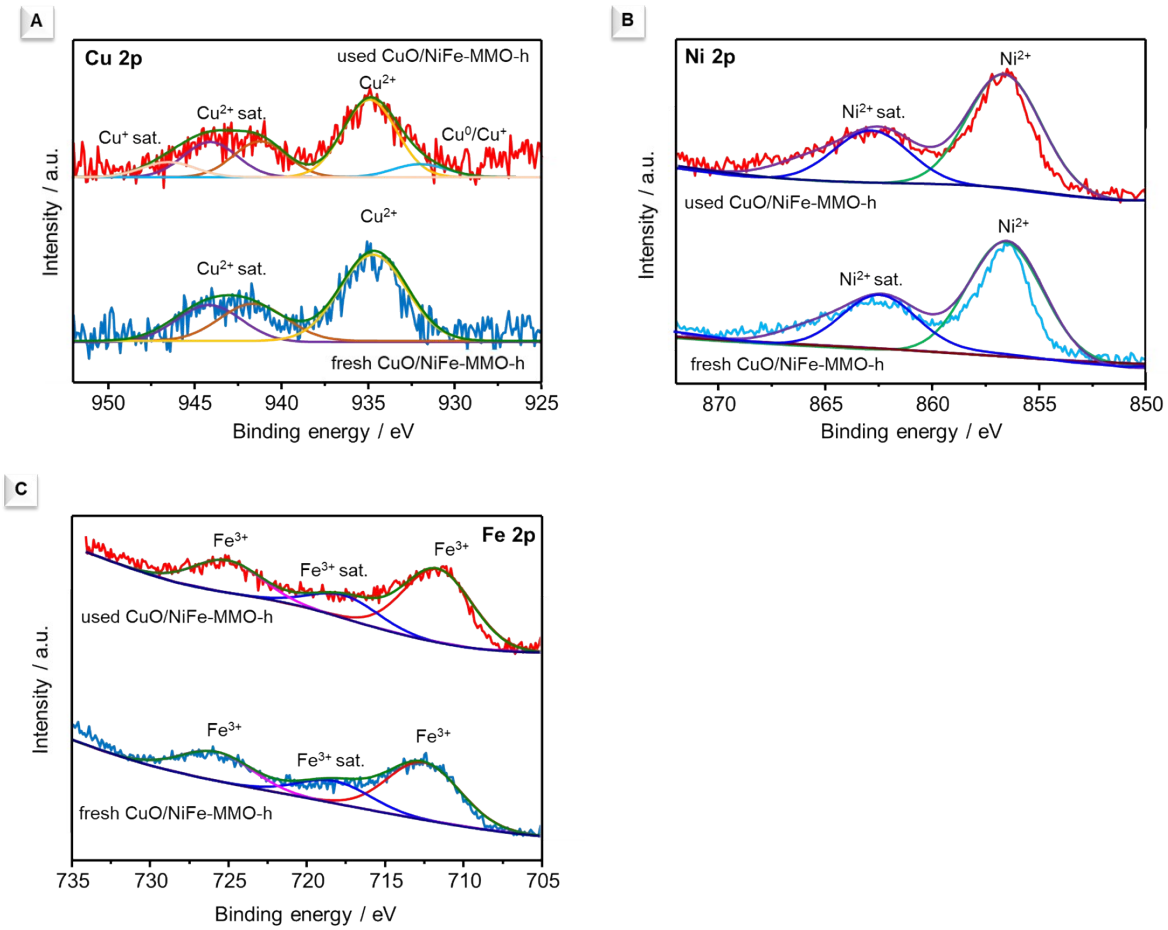

Fig. S11 XPS spectra of (A) Cu 2p, (B) Ni 2p and (C) Fe 2p for CuO/NiFe-MMO-h collected before (blue line) and after (red line) photocatalytic H_2 production reaction.

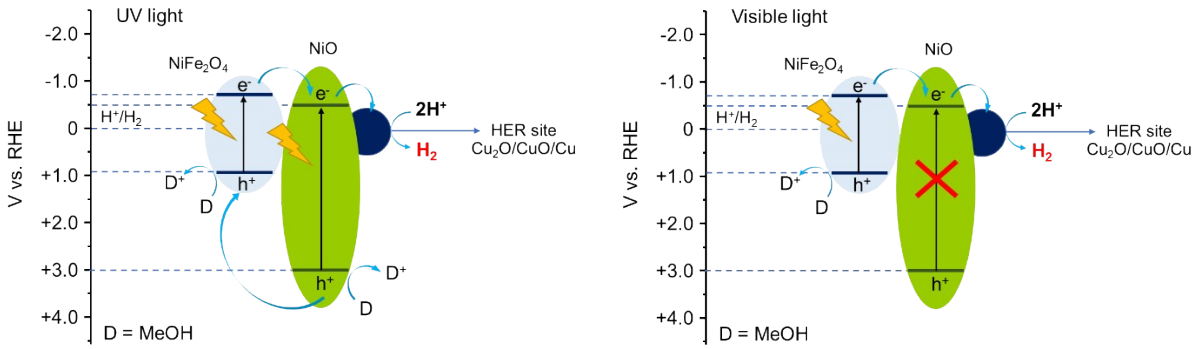

Fig. S12 Proposed photocatalytic mechanism using CuO/NiFe-MMO-h as a photocatalyst.

References

1. V. Oison, H. Ouali, C. Lambert-Mauriat and M. Freyss, *Surface science*, 2014, **622**, 44-50.
2. M. Nolan, R. Long, N. J. English and D. A. Mooney, *The Journal of chemical physics*, 2011, **134**, 224703.
3. X. Shi, Y.-F. Li, S. L. Bernasek and A. Selloni, *Surface Science*, 2015, **640**, 73-79.
4. A. C. Thenuwara, N. H. Attanayake, J. Yu, J. P. Perdew, E. J. Elzinga, Q. Yan and D. R. Strongin, *The Journal of Physical Chemistry B*, 2018, **122**, 847-854.
5. X. Yu, X. Zhang, H. Wang and G. Feng, *Applied Surface Science*, 2017, **425**, 803-810.
6. W. Zhao, M. Bajdich, S. Carey, A. Vojvodic, J. K. Nørskov and C. T. Campbell, *Acs Catalysis*, 2016, **6**, 7377-7384.
7. X. Wang, Y. Tuo, Y. Zhou, D. Wang, S. Wang and J. Zhang, *Chemical Engineering Journal*, 2021, **403**, 126297.
8. S. Sun, D. Zhang, C. Li and Y. Wang, *RSC Advances*, 2015, **5**, 21806-21811.
9. N. Zhao, L. Wang, Z. Zhang and Y. Li, *ACS applied materials & interfaces*, 2019, **11**, 42014-42020.
10. Y. Bai, B. W. Chen, G. Peng and M. Mavrikakis, *Catalysis Science & Technology*, 2018, **8**, 3321-3335.
11. Y. Liu and Z. Yang, *RSC Advances*, 2016, **6**, 68584-68591.